Supporting Information

The influence of transition metal oxides on the kinetics of Li_2O_2 oxidation for Li-O_2 batteries

Koffi P.C. Yao,[a] Yi-Chun Lu,[b] Chibueze V. Amanchukwu,[c] David G. Kwabi,[a] Marcel Risch,[a] Jigang Zhou,[d] Alexis Grimaud,[a] Paula T. Hammond,[c] Fanny Bardé,[e] and Yang Shao-Horn,*[a,b]

[a] *Department of Mechanical Engineering, Massachusetts Institute of Technology, 77 Massachusetts Avenue, Cambridge, MA 02139, USA. Email:shaohorn@mit.edu*

[b] *Department of Materials Science and Engineering, Massachusetts Institute of Technology, 77 Massachusetts Avenue, Cambridge, MA 02139, USA*

[c] *Department of Chemical Engineering, Massachusetts Institute of Technology, 77 Massachusetts Avenue, Cambridge, MA 02139, USA*

[d] *Canadian Light Source Inc., University of Saskatchewan, Saskatoon, SK S7N 0X4, CANADA*

[e] *Toyota Motor Europe, Research & Development 3, Advanced Technology 1, Hoge Wei 33 B, B-1930 Zaventem, Belgium*

Present addresses:
Author Yi-Chun Lu: Department of Mechanical and Automation Engineering, The Chinese University of Hong Kong, Hong Kong, P. R. China.

Details of perovskites synthesis

Two methods were used to obtain the perovskites investigated in the present thesis: co-precipitation and nitrates combustion. All methods have been reported previously, therefore, are described briefly below. Reference to the original work is provided.

Co-precipitation[1] was used for the synthesis of $LaCrO_3$, $LaNiO_3$ and $LaMnO_{3+\delta}$. Nitrates of lanthanum and the transition metal (99.98%, Alfa Aesar) were mixed in de-ionized water (Milli-Q water, 18 MΩ·cm) at metal molar ratio of 1:1 and total concentration of 0.2 M. The solution was subsequently titrated using an aqueous 1.2 M solution of tetramethylammonium hydroxide (100%, Alfa Aesar) resulting in precipitation. The precipitate was then filtered and collected to dry. Finally, the precipitate powder is heat treated in a tube oven at ~1000 ˚C under dry air for approximately 10 hours.

Nitrate combustion[2] was used for the synthesis of $Ba_{0.5}Sr_{0.5}Co_{0.8}Fe_{0.2}O_3$ and $LaFeO_3$. Nitrates of the rare earth and transition metal cations (Sigma Aldrich, > 99.99%) were mixed in a 2000 mL beaker at the required molar ratios of cations and total metal concentration of 0.2 M. Approximately, 0.1 M glycine was added to the mixture and homogenized using a magnetic stir plate. The mixture was heated until full evaporation of the water, followed by combustion of the solid deposit within the beaker on the heating plate. The powder was collected and heat treated under dry air at ~1000 ˚C for 24 hours in a tube furnace.

Purity of the synthesized perovskites was investigated using a PANanalytical X'Pert Pro™ X-ray diffractometer with copper K_α wavelength (λ = 1.5418 nm). All obtained materials were confirmed to be optimally pure (Fig. S1). Some minor impurities estimated below 1% of the total perovskite phase were observed for $LaCrO_3$ and $LaMnO_3$ and are not expected to influence the subsequent electrochemical studies.

Ball-milling of perovskites: All powders were ball-milled using planetary ball mill (Pulverisette 6, Fritsch Inc.) at 500 rpm for 15 hours reversing every 30 minutes. Milling reversal was preceded by a 15 minutes cooling pause. A zirconium oxide milling crucible and one-millimeter diameter zirconia milling balls were employed.

Nomenclature notes:

In the subsequent figure captions, Nafion® is used to refer to lithium exchanged Nafion® (Ion Power USA, LITHion™, 7.2 wt%). All specified component ratios in composite electrodes are mass ratios.

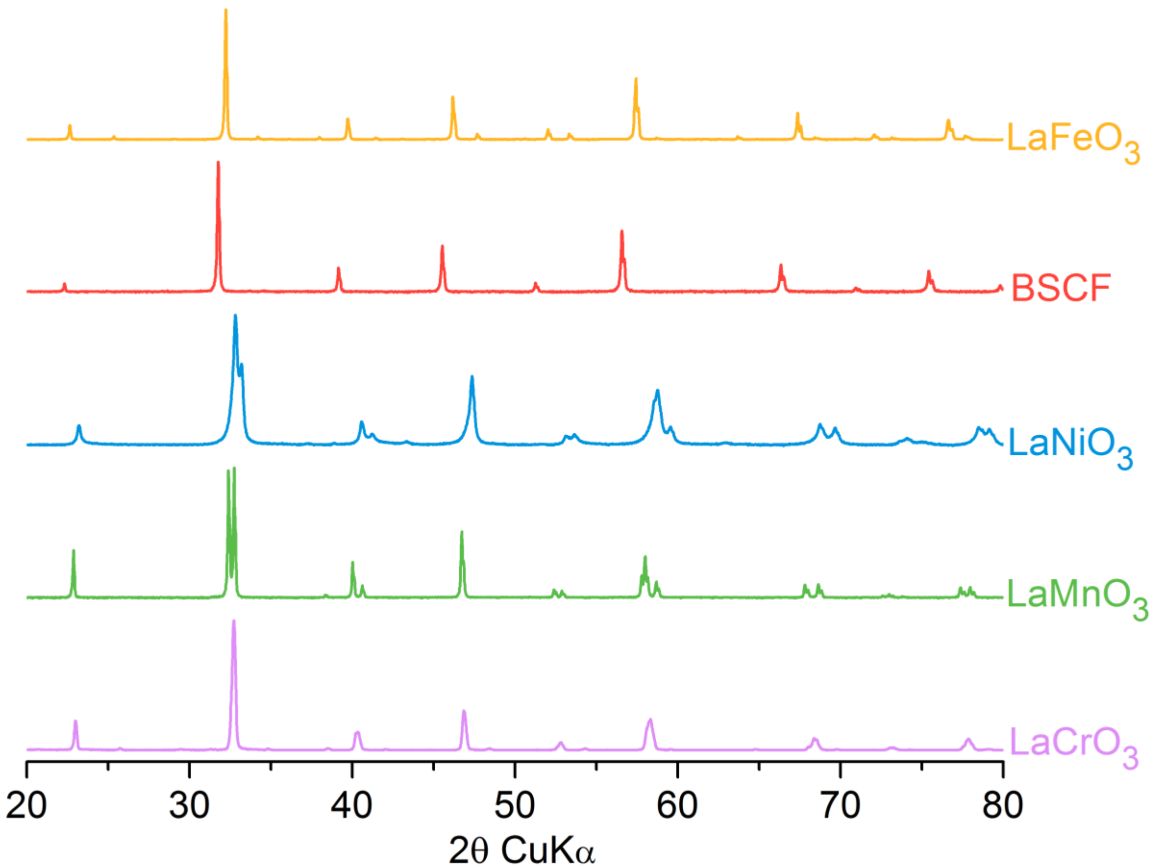

Fig. S1: Phase purity of as-synthesized perovskites investigated by X-ray diffraction. Optimal purity of each perovskite is observed. Minor impurity phases estimated to less than 1% (peaks not very visible) were detected for $LaCrO_3$ and $LaMnO_3$.

Background subtraction:

Background current (normalized to carbon mass) is subtracted from cell currents (normalized to carbon mass) in the time domain to arrive at "net currents" (see Fig. S2). Capacity is calculated by integrating the "net current" in time. Area specific current are also calculated from "net current".

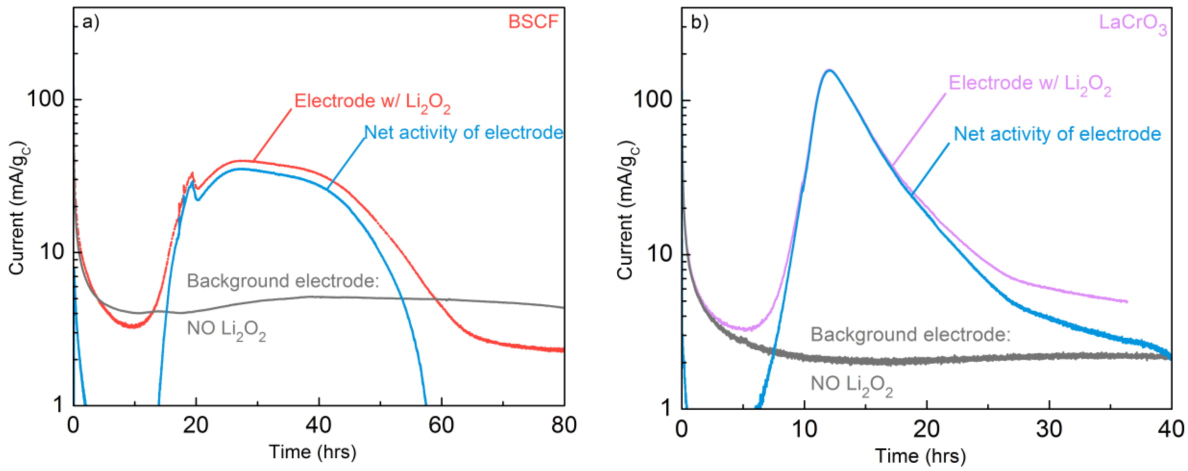

Fig. S2: Example of background subtraction performed on (a) BSCF:VC:Li_2O_2:Nafion® = 3:1:1:1 and (b) $LaCrO_3$:VC:Li_2O_2:Nafion® = 3:1:1:1 electrodes at 4.0 V_{Li}. Little change is observed in the final current (Net activity of electrode), which highlights the negligible magnitude of parasitic currents compared to actual Li_2O_2 oxidation currents. Negligible and featureless current curves of the electrode with no Li_2O_2 compared to electrode with Li_2O_2 proves that the observed performance of peroxide packed electrodes is due to effective oxidation of Li_2O_2.

SEM images of pristine and charged perovskite-catalyzed, Li_2O_2-preloaded electrodes

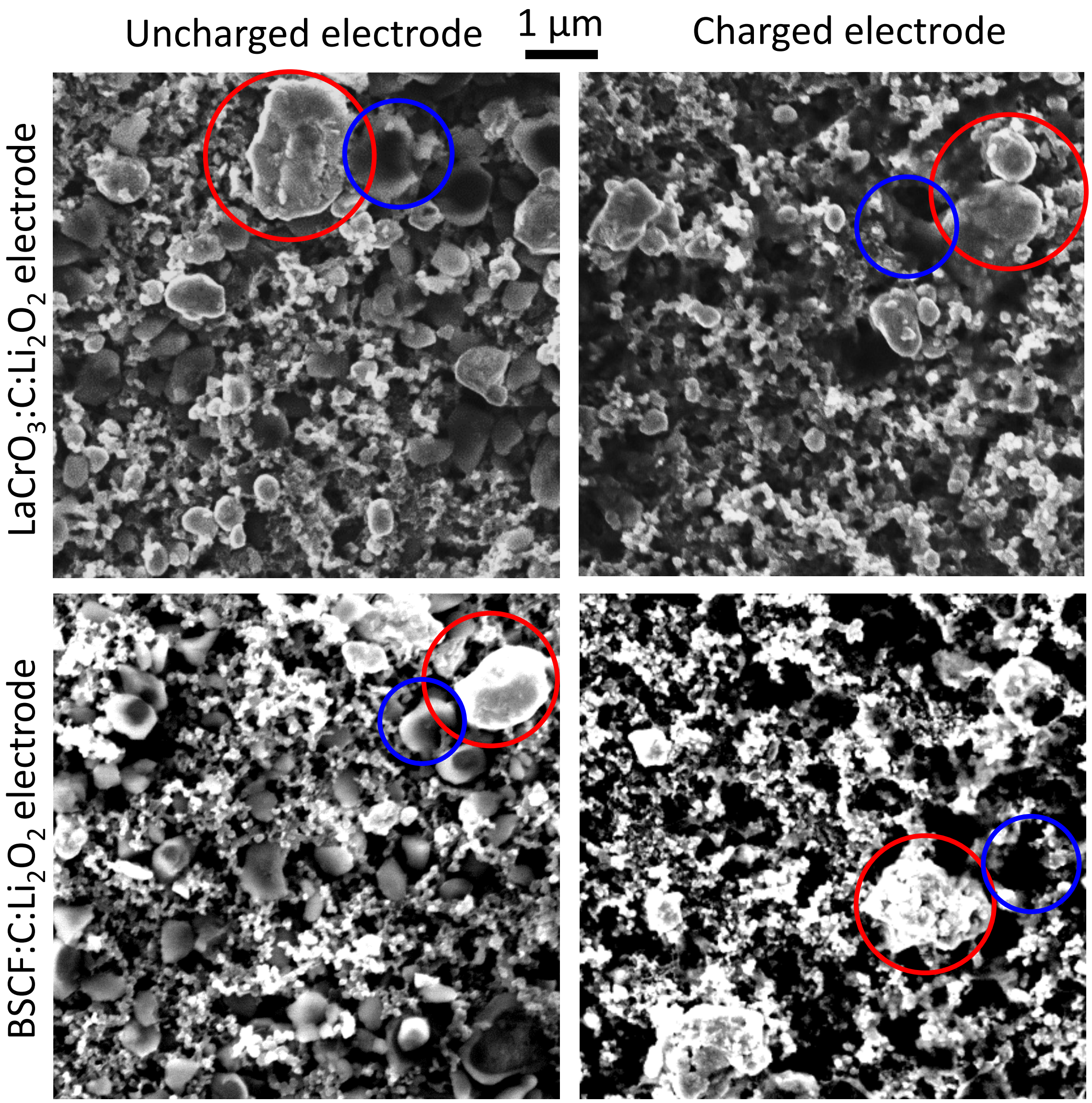

Fig. S3: SEMs of $LaCrO_3$:VC:Li_2O_2:Nafion® = 3:1:1:1 and BSCF:VC:Li_2O_2:Nafion® = 3:1:1:1 electrodes. (left): Pristine electrodes displaying Li_2O_2 and perovskite particles surrounded by carbon. (right): Charged electrodes contains no visible Li_2O_2 particles after 100% charging. Red circle: Perovskite particles location; Blue circle: Li_2O_2 particles location.

Charging curves of BSCF-catalyzed electrodes at 3.9, 4.0, and 4.1 V_{Li}

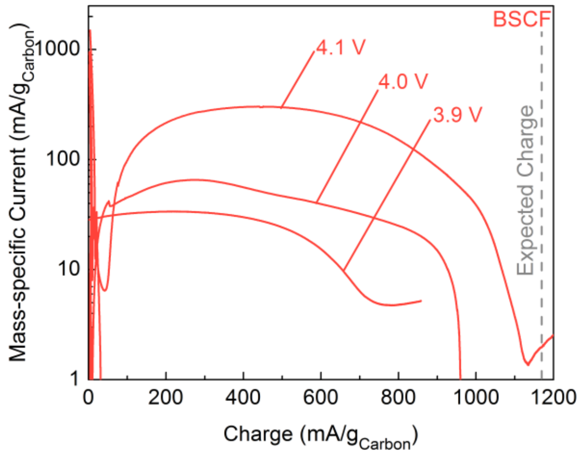

Fig. S4: Net currents normalized to carbon mass from potentiostatic charging of BSCF:VC:Li_2O_2:Nafion® = 3:1:1:1 at 4.0 V_{Li}.

Determination of cell average current

The cell's average current is calculated by integrating the "net current" in the range of 0 to 20% charge (Fig. S5) and dividing by the range of charge (mathematical average of the "net current" in the 0-20% charge range). This average is then normalized on mass or surface area bases. When reporting the average for a specific catalyst, the average current calculated per the above described method is further averaged over at least three charged cells.

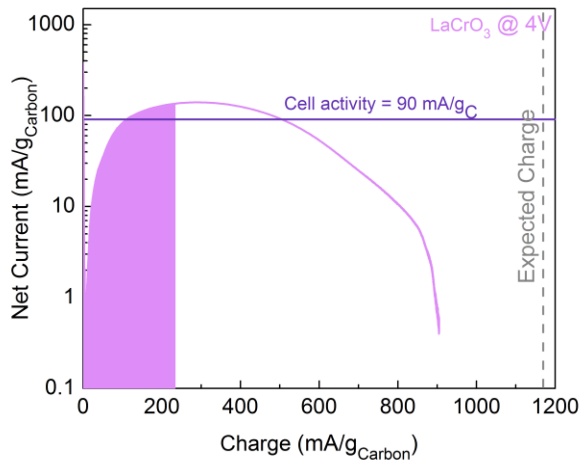

Fig. S5: Graphical representation of calculation of the mathematical average used to quantify cell activity

Plot of average current at 4.0 V_{Li} vs. eg-filling

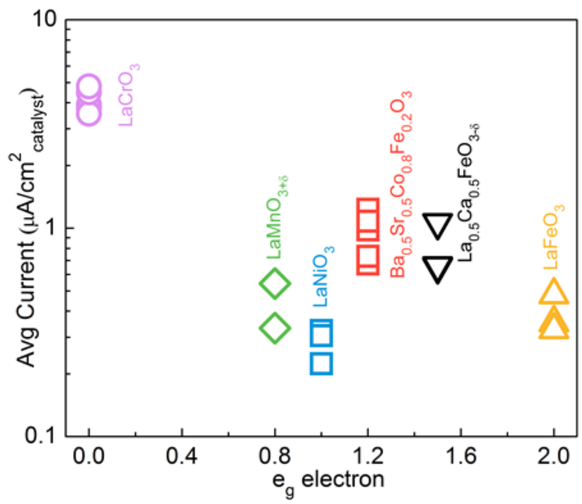

Fig. S6: Catalyst-area specific activity of Perovskite:Vulcan carbon:Li_2O_2:Nafion® = 3:1:1:1 electrodes vs. reported oxide e_g-filling. Contrary to H_2O oxidation in aqueous 0.1 M KOH[2], no volcano trend is found between e_g-filling and perovskite activity during oxidation of Li_2O_2.

SEM images of pristine and charged Cr NP-catalyzed Li_2O_2-preloaded electrodes

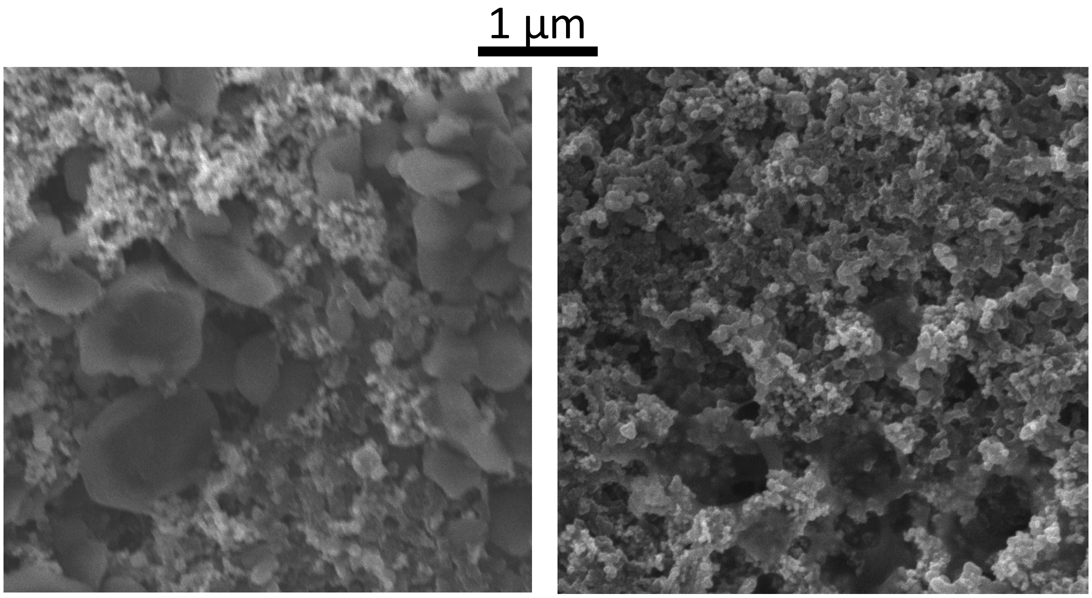

Fig. S7: SEMs of Cr:VC:Li_2O_2:Nafion® = 0.66:1:1:1 electrodes catalyzed electrodes with preloaded Li_2O_2. (left): Pristine electrodes displaying Li_2O_2 and Cr nanoparticles (Cr NP) decorating carbon surfaces. (right): Similar electrode after charging at 3.9 V_{Li} contains no visible Li_2O_2 particles after 100% charging; instead holes corresponding to the ~350 nm Li_2O_2 are observed. Small Cr NP still liter the carbon surfaces post charging.

Assessment of parasitic oxidation in Cr NP-catalyzed electrodes

1- Electrochemical assessment

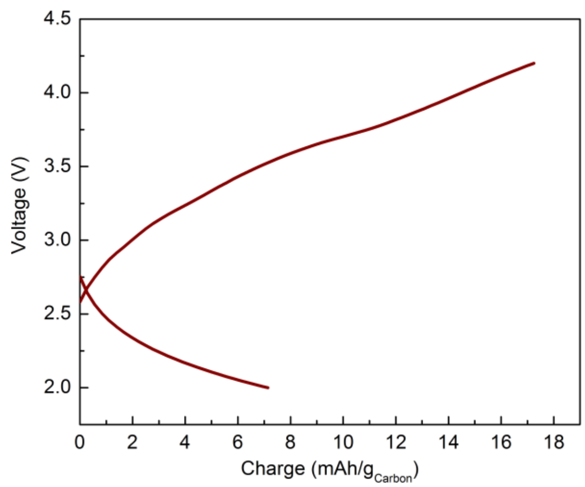

Fig. S8: Discharge and charge at 100 mA g^{-1}_{Carbon} under argon atmosphere of a Cr/C (Cr:C:Nafion® = 2:1:0.5). The output charge (< 18 mAh g^{-1}_{Carbon}) is well below the ~750 mAh g^{-1}_{Carbon} observed for the same electrode under oxygen atmosphere (Fig. 5 of main manuscript).

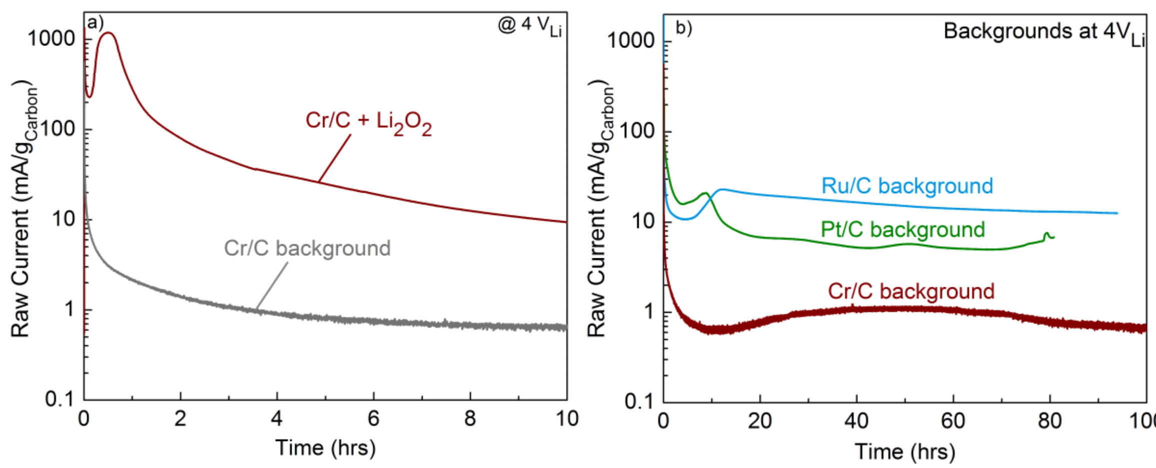

Fig. S9: (a) Potentiostatic charging profile of Cr:C:Li_2O_2:Nafion® = 0.66:1:1:1 compared to that of its background (Li_2O_2-free) at 4 V_{Li}. The small average current (~1 mA g^{-1}_{Carbon}) of the background compared to that of the Li_2O_2-preloaded electrode (~1000 mA g^{-1}_{Carbon}) indicates negligible parasitic electrolyte oxidation in presence of Cr NP. (b) Comparison of background oxidation currents at 4 V_{Li} in presence of Cr, Pt and Ru (Cr,Pt,Ru:C:Nafion® = 0.66:1:0.5) without Li_2O_2. The observed parasitic oxidation current is a factor of 10 higher on the surfaces of noble metal Pt and Ru.

2- Spectroscopic assessment

To investigate the extent of parasitic electrolyte decomposition accompanying the enhanced Li_2O_2 oxidation in presence of Cr NP, solid deposits on electrodes post-charging at 3.9 V_{Li} and 4.0 V_{Li} were probed using nuclear magnetic resonance (NMR) spectroscopy. A Bruker AVANCE 400 NMR spectrometer was used to collect all ^{1}H NMR data. Lithium formate (HCOOLi) and acetate (CH_3COOLi) are reported as the main decomposition products of ether solvents.[3, 4] The experimental procedure used to probe these products is reported elsewhere,[4] and is briefly described below:

- C:Li_2O_2:Nafion® = 1:1:1, Cr:C:Li_2O_2:Nafion® = 0.66:1:1:1, and Cr:C:Nafion® = 0.66:1:1 electrodes are charged at either 3.9 V_{Li} or 4.0 V_{Li}. Representative charge profiles are shown in Fig. 3 of the main manuscript.
- All electrodes are triple washed with acetonitrile to selectively remove inorganic lithium salts such as $LiClO_4$ used in the electrolyte. Organic salts such as HCOOLi and CH_3COOLi do not dissolve in acetonitrile.
- Electrodes are then immersed in 0.65 mL D_2O for 4 hours to dissolve any organic salts from electrolyte decomposition.
- The D_2O wash is collected for ^{1}H NMR

Assignment of NMR peaks for HCOOD (representing HCOOLi) and CH_3COOD (representing CH_3COOLi) are based on the works of Freunberger et al.[3] and Black et al.[4] The following results are gathered from the NMR spectra shown in Fig. S10 below:

C:Li_2O_2:Nafion® : ^{1}H NMR (400 MHz, D_2O) δ ppm 8.47 (s, 1H), 2.08 (s, 3H)

Cr:C:Li_2O_2 at 3.9V : ^{1}H NMR (400 MHz, D_2O) δ ppm 8.45 (s, 1H), 1.91 (s, 3H)

Cr:C:Li_2O_2 at 4V: ^{1}H NMR (400 MHz, D_2O) δ ppm 8.45 (s, 1H)

Cr:C at 4V: No peaks corresponding to HCOOLi or CH_3COOLi

It is clear that formation of HCOOLi and CH_3COOLi occurs irrespective of the presence or absence of Cr NP in all electrodes containing Li_2O_2. Comparison of spectral intensities of the HCOOD and CH_3COOD peaks between Cr NP electrodes and carbon-only electrodes suggests no enhanced electrolyte decomposition in presence of Cr NP. Background electrodes of Cr NP without Li_2O_2 charged at 4.0 V_{Li} show no electrolyte decomposition products, which confirms the relative benign effect of Cr NP on the dimethoxyethane electrolyte seen in Fig. S9.

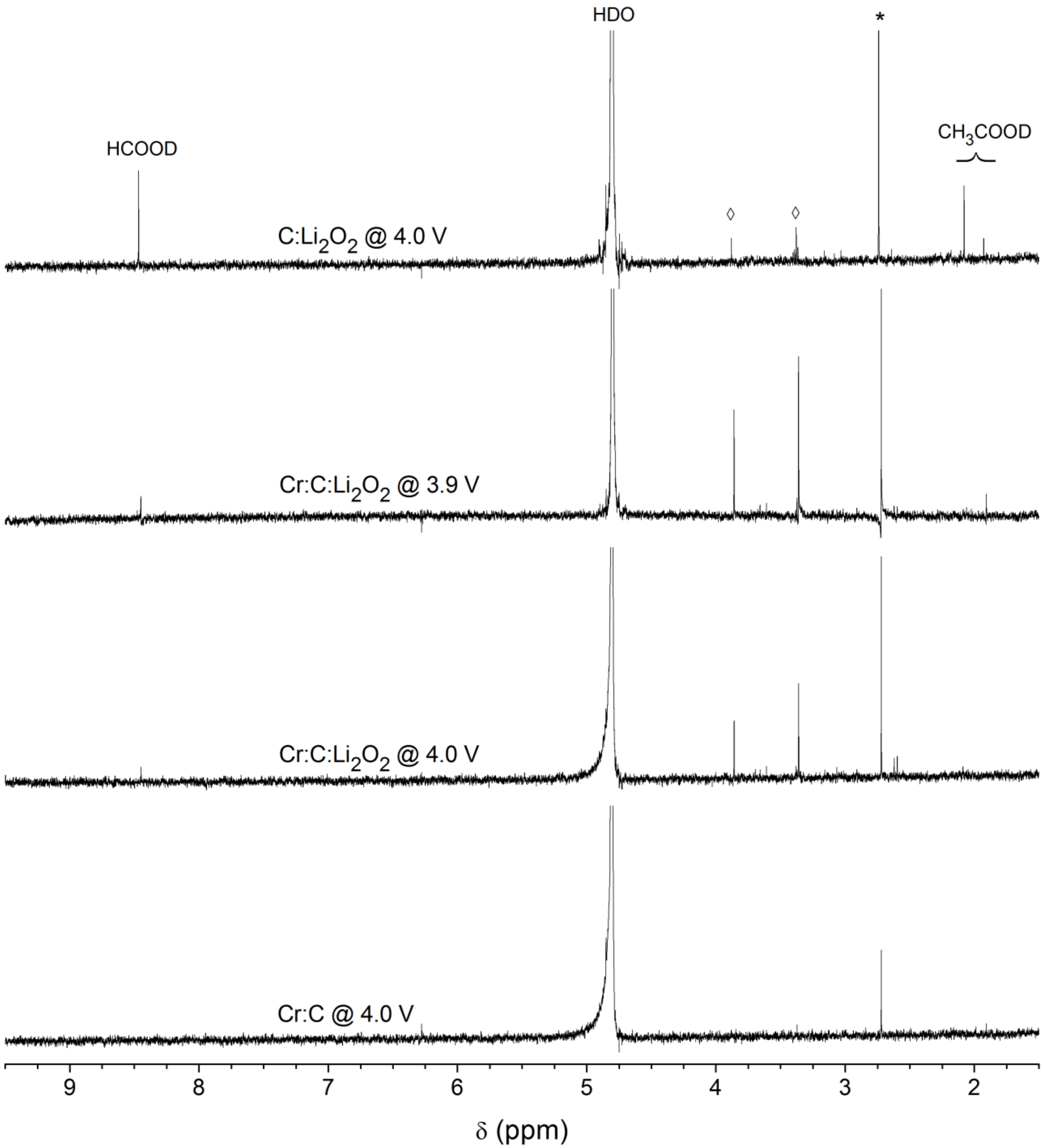

Fig. S10: (top to bottom) NMR spectra of C:Li_2O_2:Nafion® = 1:1:1 charged at 4.0 V_{Li}, Cr:C:Li_2O_2:Nafion® = 0.66:1:1:1 charged at 3.9 V_{Li}, Cr:C:Li_2O_2:Nafion® = 0.66:1:1:1 charged at 4.0 V_{Li} and Cr:C:Nafion® = 0.66:1:1 polarized at 4.0 V_{Li}. Unidentified peaks at δ = 3.86 and 3.36 ppm (◊) appear tied to the presence of Li_2O_2 as they are absent from the Cr:C:Nafion® without Li_2O_2. These unidentified peaks were also noted in the work by Freunberger et al.[3] The peak at δ = 2.72 (*) is tied to the presence of carbon as it is observed in all electrodes with and without chromium and was not observed in electrodes without carbon (spectrum not shown).

Discharge product in discharged Cr NP-catalyzed Li-O_2 cells

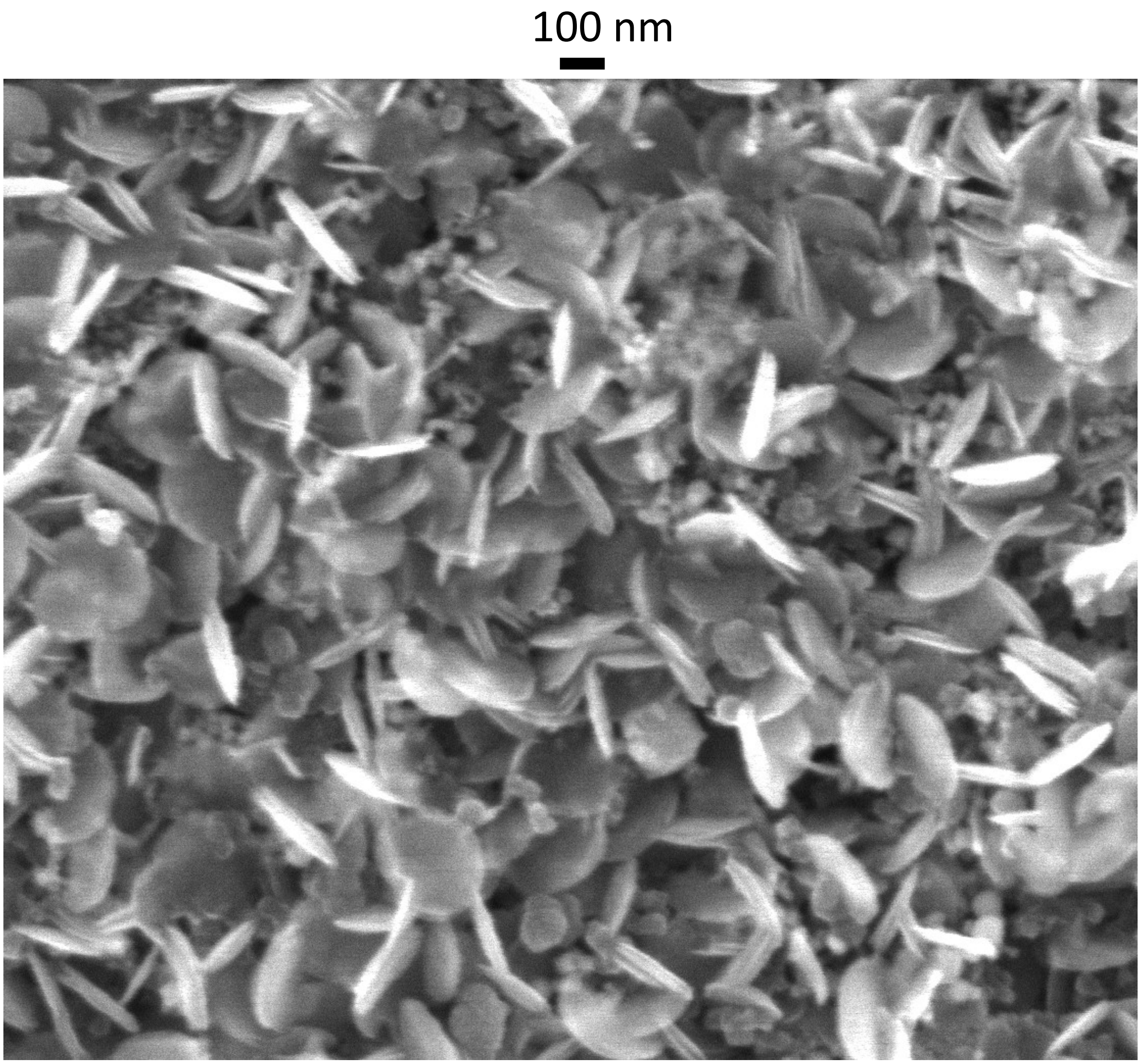

Fig. S11: SEMs of discharged Cr/C (Cr:C:Nafion® = 2:1:0.5) Li-O_2 electrode. ~200 nm particles of Li_2O_2 confirmed by XRD (Fig. S12) are visible and covering the carbon structure. Smaller ~40 nm point-particles are Cr NP.

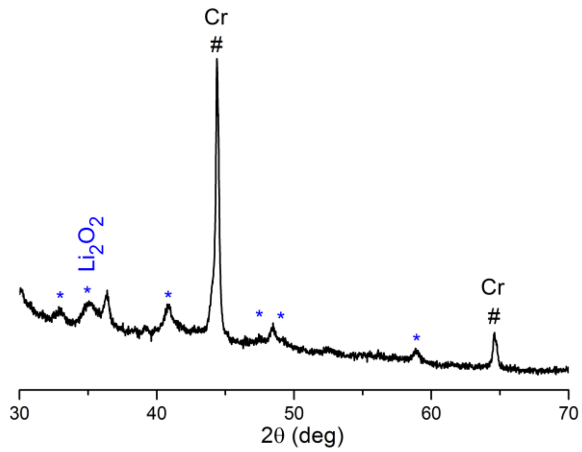

Fig. S12: Post-discharge XRD of Cr/C (Cr:C:Nafion® = 2:1:1) Li-O_2 electrode. The discharge product is confirmed to be crystalline Li_2O_2.

X-ray absorption analysis of carbon-free Cr NP-catalyzed electrodes

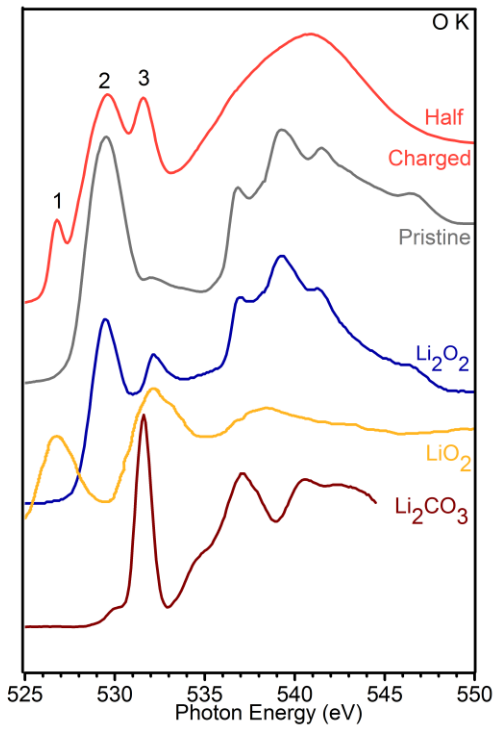

Fig.S13: Comparison of O K-edge XANES spectra of the pristine and half-charged Cr:Li_2O_2 electrodes to reference spectra of Li_2CO_3, Li_2O_2[16, 40] and LiO_2[5]. Energies are calibrated to the spectral features of Li_2O_2 in the as-made Cr:Li_2O_2 electrode.

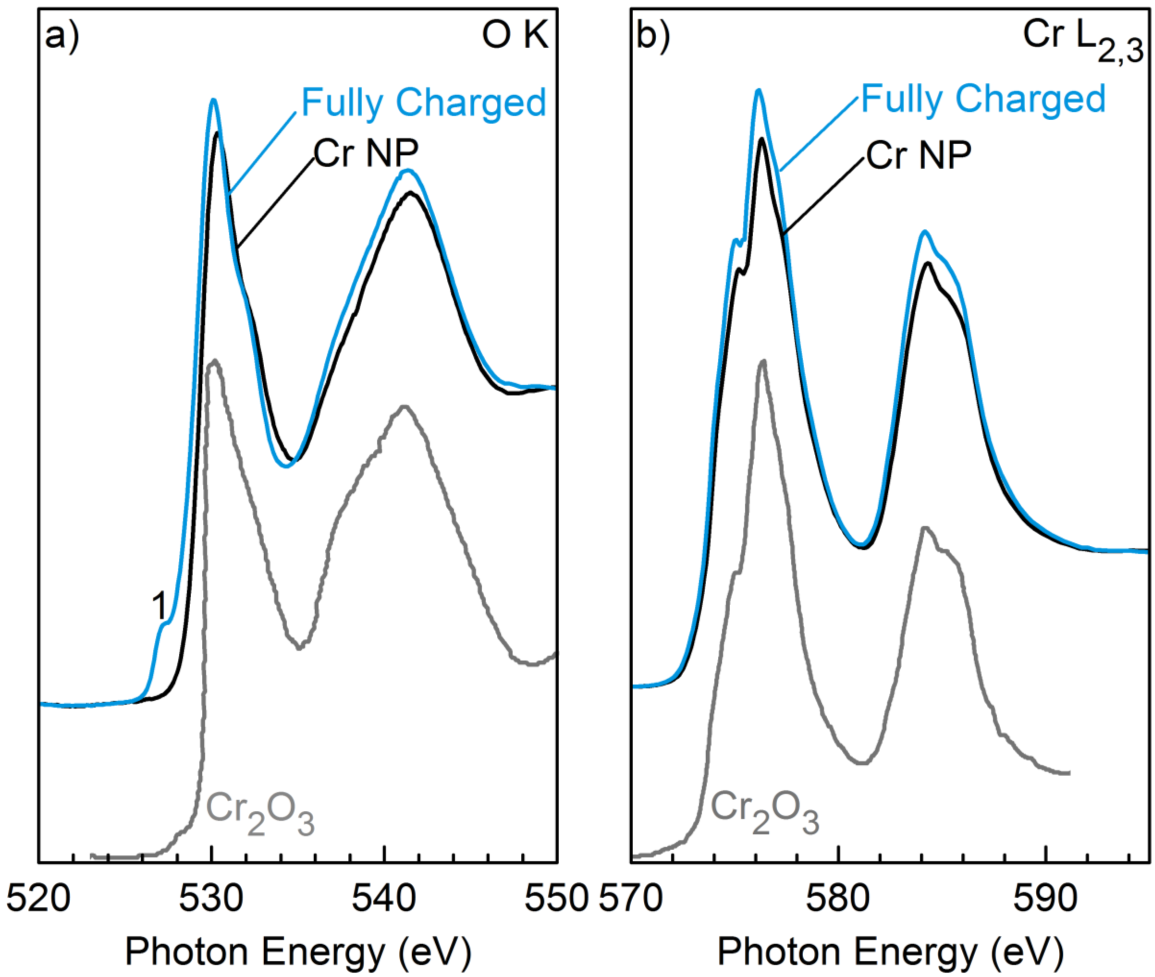

Fig. S14: Comparison of O K-edge XANES spectra of the as-purchased and fully-charged Cr:Li_2O_2 electrodes to reference spectra of Cr_2O_3.[6, 7]

Table S1: Literature values for Li_2O_2 oxidation activities under various cell conditions

Catalyst	Electrolyte used	Rate (mA g^{-1}_{Carbon})	Rate (mA g^{-1}_{Li2O2})*	Rate (μA cm^{-2}_{Carbon})	Rate (μA cm^{-2}_{Cat})	Rate (μA $cm^{-2}_{Carbon+Cat}$)	Charging voltage (V)	Cathode structure
Pt/VC	0.1 M $LiClO_4$ 1,2 Dimethoxyethane	70	70	0.070	0.114	0.043	~3.6	Li_2O_2-prefilled ($VC:Catalyst:Li_2O_2$ = 1:0.66:1)[8]
Ru/VC				0.070	0.088	0.039	~3.6	
Au/VC				0.070	0.482	0.061	~4.2	
Vulcan Carbon (VC)				0.070	0.070	0.035	~4.1	
KB/Acid leached $Na_{0.44}MnO_2$	1 M $LiPF_6$ TEGDME	70	7.4	0.009	0.255	0.008	~3.8	Li-O_2 cell (KB:Catalyst = 1:0.4)[9]
KB/Pristine $Na_{0.44}MnO_2$			14	0.009	0.384	0.008	~4.0	
Ketjen black (KB)			41	0.009	0.009	0.008	~4.1	
KB/Lead ruthenate	1 M $LiPF_6$ TEGDME	70	14	0.009	0.106	0.008	~4.0	Li-O_2 cell (KB:Catalyst = 1:1)[10]
KB/Bismuth ruthenate			14	0.009	0.068	0.008	~4.0	
Ketjen Carbon (KB)			27	0.009	0.009	0.004	~4.2	
KB/ $La_{1.7}Ca_{0.3}Ni_{0.75}Cu_{0.25}O_4$	1 M $LiPF_6$ TEGDME	20	67	0.008	1.811	0.008	~3.6	Li_2O_2-prefilled ($KB:Catalyst:Li_2O_2$ = 1:0.3:0.3)[11]
Super P (No catalyst)	0.1M $LiClO_4$, DMF	70	54	0.113	0.113	0.113	~3.6	$LiFePO_4$-O_2 cell[12]
Super P (No catalyst)	0.1M $LiClO_4$, DMSO	70	164	0.113	0.113	0.113	~4.1	Li-O_2 cell[13]

Super P/Gold nano composite electrode	0.1M $LiClO_4$, DMSO	70	164	0.113	1.120	0.103	~3.8	Li-O_2 cell (Super P:PTFE:Au = 8:1:1)[13]
Nanoporous Gold	0.1M $LiClO_4$, DMSO	500 mA/g_{Au}	1947	N/A	1.000	1.000	~3.5	Li-O_2 cell[13]

* Normalized to the weight of Li_2O_2 (preloaded or electrochemically-formed) right before charging

Surface areas of catalyst particles

Table S2: SEM calculated particles size and surface areas of the perovskites investigated.

Oxide	$d_{v/a}$ (nm)	Surface Area (m^2/g_{ox})
BSCF	647.22	1.596
$LaMnO_3$	574.53	1.821
$LaNiO_3$	206.11	4.108
$LaFeO_3$	454.05	1.981
$LaCrO_3$	951.08	0.946

Extraction of the surface areas from SEM images was done following the same procedure detailed by Suntivich et al.[2] The following formula is employed:

$$A_s = \frac{6}{\rho \cdot d_{v/a}} \; with \; d_{v/a} = \frac{\sum d^3}{\sum d^2}$$

Where d is the average diameter of particles approximated as spherical. d is calculated based on the measured surface area (using ImageJ image processing software, offered by NIH) of particles observed. The same procedure is used by Harding et al.[8] in extracting the surface areas of Pt, Ru and Au in Pt/C, Ru/C, and Au/C catalysts.

In the case of Cr-nanoparticles and Cr_2O_3, surface area was obtained using Brunauer–Emmett–Teller (BET) measurements using nitrogen adsorption/desorption. The measurement yielded a surface area of ~24 $m^2/g_{Cr\ NP}$ for Cr NP, in good agreement with the values of (20-30 $m^2/g_{Cr\ NP}$) reported by the manufacturer (US Research Nanomaterials Inc.). The surface area of Cr_2O_3 was measured at ~20 m^2/g_{Cr2O3}.

REFERENCES

1. J. Suntivich, H. A. Gasteiger, N. Yabuuchi, H. Nakanishi, J. B. Goodenough and Y. Shao-Horn, *Nat. Chem.*, 2011, **3**, 546-550.
2. J. Suntivich, K. J. May, H. A. Gasteiger, J. B. Goodenough and Y. Shao-Horn, *Science*, 2011, **334**, 1383-1385.
3. S. A. Freunberger, Y. Chen, N. E. Drewett, L. J. Hardwick, F. Bardé and P. G. Bruce, *Angew. Chem. Int. Ed.*, 2011, **50**, 8609-8613.
4. R. Black, S. H. Oh, J. H. Lee, T. Yim, B. Adams and L. F. Nazar, *J. Am. Chem. Soc.*, 2012, **134**, 2902-2905.
5. M. W. Ruckman, J. Chen, S. L. Qiu, P. Kuiper, M. Strongin and B. I. Dunlap, *Phys. Rev. Lett.*, 1991, **67**, 2533-2536.
6. T. Schedel-Niedrig, *Fresenius J. Anal. Chem.*, 1998, **361**, 680-682.
7. M. O. Figueiredo, A. C. dos Santos, M. J. Carmezim, M. Abbate, F. M. F. de Groot, H. Petersen and W. Braun, *Analyst*, 1994, **119**, 609-611.
8. J. R. Harding, Y. C. Lu, Y. Tsukada and Y. Shao-Horn, *Phys. Chem. Chem. Phys.*, 2012, **14**, 10540-10546.
9. J.-H. Lee, R. Black, G. Popov, E. Pomerantseva, F. Nan, G. A. Botton and L. F. Nazar, *Energy Environ. Sci.*, 2012, **5**, 9558-9565.
10. S. H. Oh and L. F. Nazar, *Adv. Energy Mater.*, 2012, **2**, 903-910.
11. K.-N. Jung, J.-I. Lee, W. B. Im, S. Yoon, K.-H. Shin and J.-W. Lee, *Chem. Commun.*, 2012, **48**, 9406-9408.
12. Y. Chen, S. A. Freunberger, Z. Peng, F. Bardé and P. G. Bruce, *J. Am. Chem. Soc.*, 2012, **134**, 7952-7957.
13. Z. Peng, S. A. Freunberger, Y. Chen and P. G. Bruce, *Science*, 2012, **337**, 563-566.